Separation of Hydrogen Mixtures by a Two-Bed Pressure Swing Adsorption Process Using Zeolite 5A

Jaeyoung Yang and Chang-Ha Lee*

Department of Chemical Engineering, Yonsei University, Shinchon-dong, Seodaemoon-ku, Seoul 120-749, Korea

Jay-Woo Chang

Sunkyong Engineering & Construction Limited, Kwanhun-dong, Chongro-ku, Seoul 110-300, Korea

A study on a two-bed six-step pressure swing adsorption (PSA) process using zeolite 5A was performed experimentally and theoretically for bulk separation of H_2/CO and H_2/CH_4 systems (70/30 vol %) as major components in coke oven gas. When the pressure is cycled between 1 and 11 atm at ambient temperatures, 70% H_2 in the feed could be concentrated to 99.99% in the product with a recovery of 75.87% in the H_2/CO mixture and 80.38% in the H_2/CH_4 mixture. The effects of adsorption pressure, *P*/*F* ratio, adsorption/purge step time, and pressure equalization step time were investigated experimentally. If the product end of an adsorption bed was not contaminated during the adsorption and depressurizing pressure equalization steps, elongation of both the adsorption and purge steps gave good adsorbent productivity and recovery without any decrease in purity. Certain elongations of step time in the pressure equalization step resulted in a better performance of a PSA process. When the H_2 mole fraction of effluent stream during the pressure equalization step was not high, the initial H_2 purity of the adsorption step was not good because of the contamination of the product end section. These results were analyzed by a mathematical model incorporating heat and momentum balances.

Introduction

The pressure swing adsorption (PSA) process has become a widely used unit operation for gas separation or purification. Due to an increasing demand of hydrogen for petroleum refinery and petrochemical processing, a strong economic motivation has prompted the development of processes to recover hydrogen from steam reformer off gas, catalytic reformer off gas, and ethylene plant effluent gas. The H_2 recovery PSA process widely used in the chemical and petroleum refining industry is one of typical multibed PSA processes incorporating many PSA steps in various ways. Another promising use of the established H_2 PSA process is H_2 recovery from coke oven gas (COG). COG is composed of about 60% hydrogen, 25% methane, 8% carbon monoxide, and a small amount of carbon dioxide, nitrogen, oxygen, etc. In these processes, an adsorption bed is made of several adsorbents such as alumina, activated carbon, and zeolite because in most cases some impurities should be pretreated first before any major impurities are adsorbed in the main adsorbent section (Chlendi and Tondeur, 1995; Yang, 1987). As zeolite 5A is widely used as an adsorbent at the main section of the adsorption bed in a PSA process, it is important to study a PSA process using zeolite 5A.

To understand and develop the H_2 PSA process, H_2 PSA was extensively studied by many researchers. Using activated carbon, Yang and co-workers (Yang and Doong, 1985; Cen and Yang, 1986; Doong and Yang, 1986) have reported the separation of H_2/CH_4/CO_2 and H_2/CO mixtures by a one-bed PSA process. They studied the effects of many operating parameters and the kinetics of adsorption by which the theoretical PSA model was classified by an equilibrium model, linear driving force (LDF) model, monodisperse pore diffusion model, and a surface diffusion model. Doong and Yang (1987) also presented discussion on the relative importance of micropore and macropore diffusion in a one-bed PSA using zeolite 5A through a simulated prediction in a 50/50 mixture of H_2 and CH_4. Kumar (1994) carried out a numerical study on a multibed H_2 PSA process to separate a H_2/CH_4 mixture with a Ca-exchanged A zeolite. In his study, an optimum purge quantity was determined in the process where the internal gas stream, instead of a part of a product stream, was utilized to purge the used bed. Recently, Lee and co-workers (Kim et al., 1995; Yang et al., 1995) studied the experimental and theoretical results of H_2 recovery from H_2/CO and H_2/CO_2 mixtures by a one-bed PSA process with zeolite 5A. In these studies, zeolite 5A was successfully used to obtain a hydrogen product of high purity.

In the present study, two kinds of hydrogen mixtures which include 30 vol % CO or CH_4 as a major impurity of COG were separated by a two-bed PSA process employing zeolite 5A as an adsorbent. Experiments were performed for a bulk separation of H_2 mixtures with a goal of producing H_2 of high purity. The effects of typical operating parameters on a PSA performance, such as adsorption pressure, *P*/*F* ratio, and several step times including adsorption/purge and pressure equalization steps, were studied experimentally. To develop the understanding of this process, the effects of these operating parameters on the performance of a PSA process were analyzed by a mathematical model.

Apparatus and Material

The characteristics of an adsorption bed and adsorbent are shown in Table 1. The adsorbent used in this study was zeolite 5A (4 × 8 mesh spherical bead) manufactured by Davison Chemical Division of W.R. Grace Company. Moisture-free commercial gas mixtures (H_2/CO and H_2/CH_4, 70/30 vol %) were used as feed gases.

* Author to whom correspondence should be addressed. E-mail: leech@bubble.yonsei.ac.kr.

S0888-5885(96)00728-2 CCC: $14.00

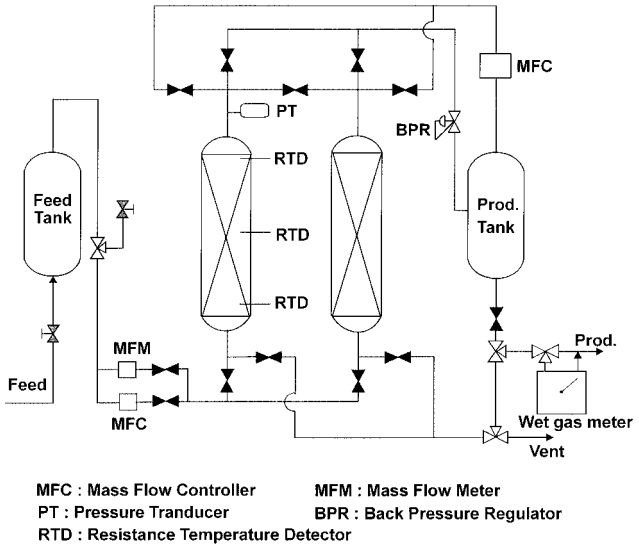

Figure 1. Schematic diagram of a two-bed PSA system.

Table 1. Characteristics of Adsorption Bed and Adsorbent

Adsorption Bed	
bed length	$L = 100$ cm
bed inside radius	$R_{Bi} = 2.2$ cm
bed outside radius	$R_{Bo} = 2.55$ cm
wall heat capacity	$C_{pw} = 0.12$ cal/g·K
bulk (bed) density	$\rho_B = 0.795$ g/cm^3
external void fraction	$\epsilon = 0.315$
total void fraction	$\alpha = 0.76$
Adsorbent	
pellet size	4−8 mesh (spherical)
average pellet size	$R_p = 1.57$ mm
pellet density	$\rho_p = 1.16$ g/cm^3
heat capacity	$C_{ps} = 0.22$ cal/g·K

The adsorption isotherms of pure H_2, CO, and CH_4 were measured at three different temperatures (293, 303, and 313 K) by using a high-pressure volumetric apparatus. This apparatus consists of two stainless steel vessels—a doser cell and an adsorber cell. The pressure variations of these cells were measured by pressure transmitters (Heise, 621). The adsorbent was regenerated at every experiment at 623 K in a furnace.

A schematic diagram of a two-bed PSA unit used in this study is shown in Figure 1. The adsorption bed is 100 cm long with 2.2 cm i.d. Three RTDs were installed at 10, 50, and 80 cm from the feed end to measure the temperature inside an adsorption bed. Feed and purge flow rates were controlled by mass flow controllers (Hastings, HFC-202E). Recovery was calculated by measuring the amount of gas flowing into and out of a PSA system using a mass flowmeter (Hastings, HFM-201) and a wet gas meter (Shinagawa, W-NK-1B). Especially, there are two branches in the feed line to supply the feed during pressurization and adsorption steps, respectively. The feed line on which a mass flowmeter was installed was used to measure the flow rate during a feed pressurization step. The other feed line on which another mass flow controller was installed was used to control the feed flow rate during an adsorption step. Therefore, in the case of using a single feed line, the pressure drop which could be caused by a mass flow controller could be excluded. As a result, the pressurization step time could be shortened, and thus, the total cycle time was reduced. The metering valve installed at a pressure equalization line was used to control the flow rate and the step time during a pressure equalization step. Gas samples were taken from the light and heavy product lines and were analyzed with a thermal conductivity detector (HP, GC 5890 II).

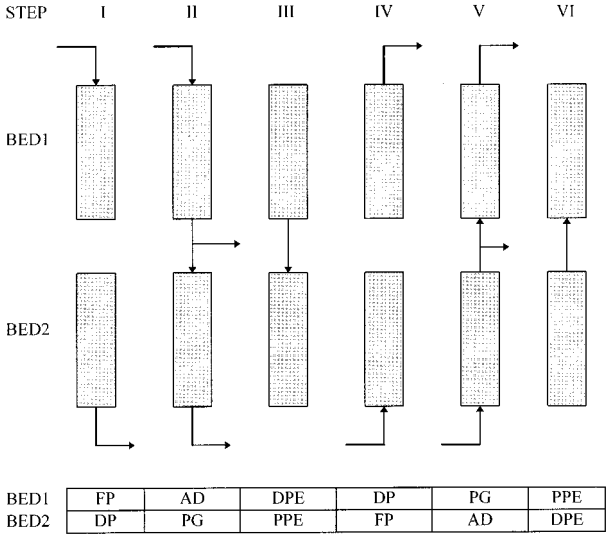

BED1	FP	AD	DPE	DP	PG	PPE
BED2	DP	PG	PPE	FP	AD	DPE

FP: Feed Pressurization, AD: Adsorption, DPE: Depressurizing Pressure Equalization, DP: Depressurization, PG: Purge, PPE: Pressurizing Pressure Equalization

Figure 2. Cycle sequence of a two-bed PSA process.

PSA Process Description

A two-bed six-step PSA process cycle to produce high-purity hydrogen from two kinds of binary mixtures containing 30% CO or CH_4 and 70% H_2 was experimented and simulated. The PSA cycle consisted of the following steps: (i) feed pressurization of a partially pressurized bed during a previous pressurizing pressure equalization step, (ii) high-pressure adsorption step, (iii) depressurizing pressure equalization step, (iv) countercurrent depressurization step, (v) purge step with a part of a light product, and (vi) pressurizing pressure equalization step. The step sequence for the process and a simple flow diagram were illustrated in Figure 2. The effects of various operating parameters on the PSA performance were investigated with a fixed feed flow rate of 2 L/min. The experiment was done at room temperature (293 ± 2 K) under the nonisothermal condition, and a slight change in the room temperature had no great effect on the results of the process.

To design a PSA process of high purity and recovery, several pressure equalization steps are needed, involving many adsorption beds. However, in this study, there was just one pressure equalization step because it investigated a two-bed PSA system. Moreover, a great amount of feed was needed for the final pressurization of an adsorption step, and a great amount of gas was released into the air during the depressurization step. Therefore, it was impossible to achieve high recovery.

Mathematical Model

A mathematical model including mass, energy, and momentum balance was constructed to develop a complete nonisothermal PSA model with the following assumptions: (i) the flow pattern is described by the axially dispersed plug flow model, (ii) thermal equilibrium is assumed between fluid and particles, (iii) the mass transfer rate is represented by a linear driving force (LDF) model, (iv) the gas phase behaves as an ideal gas mixture, and (v) radial concentration and temperature gradients are negligible.

Applying an ideal gas law, the component mass balance and overall mass balance for the bulk gas phase of an adsorption bed can be written as follows:

$$-D_L\frac{\partial^2 y_i}{\partial z^2}+\frac{\partial y_i}{\partial t}+u\frac{\partial y_i}{\partial z}+\frac{RT}{P}\frac{1-\epsilon}{\epsilon}\rho_p\left(\frac{\partial \bar{q}_i}{\partial t}-y_i\sum_{j=1}^{n}\frac{\partial \bar{q}_j}{\partial t}\right)=0 \quad (1)$$

$$-D_L\frac{\partial^2 P}{\partial z^2}+\frac{\partial P}{\partial t}+P\frac{\partial u}{\partial z}+u\frac{\partial P}{\partial z}-\frac{P}{T}\left(-D_L\frac{\partial^2 T}{\partial z^2}+\frac{\partial T}{\partial t}+u\frac{\partial T}{\partial z}\right)+\frac{1-\epsilon}{\epsilon}\rho_p RT\sum_{j=1}^{n}\frac{\partial \bar{q}_j}{\partial t}=0 \quad (2)$$

The energy balance for the gas and solid phases of an adsorption bed is given by

$$-\epsilon K_L\frac{\partial^2 T}{\partial z^2}+(\alpha\rho_g C_{p,g}+\rho_B C_{p,s})\frac{\partial T}{\partial t}+\rho_g C_{p,g}\epsilon u\frac{\partial T}{\partial z}-\rho_B\sum_i^n Q_i\frac{\partial \bar{q}_i}{\partial t}+\frac{2h_i}{R_{Bi}}(T-T_w)=0 \quad (3)$$

Since the diameter of the adsorption bed used in this study was rather small, the effect of heat transfer in the metallic bed wall could not be neglected. Therefore, another energy balance for the wall of an adsorption bed was constructed with further assumption of neglecting axial conduction in the wall:

$$\rho_w C_{pw} A_w\frac{\partial T_w}{\partial t}=2\pi R_{Bi}h_i(T-T_w)-2\pi R_{Bo}h_o(T_w-T_{atm}) \quad (4)$$

where $A_w=\pi(R_{Bo}^2-R_{Bi}^2)$ and T_w = the wall temperature of the column. However, if a larger diameter adsorber is used, this equation may be neglected.

The steady-state momentum balance in a bed was given by Ergun's equation:

$$-\frac{dP}{dz}=a\mu u+b\rho u^2 \quad (5)$$

where

$$a=\frac{150}{4R_p^2}\frac{\epsilon(1-\epsilon)^2}{\epsilon^3}$$

and

$$b=1.75\frac{\epsilon^2(1-\epsilon)^2}{2R_p\epsilon^3}$$

The sorption rate into the adsorbent, $\partial\bar{q}_i/\partial t$, could typically be described by an LDF model. The LDF model can be described by

$$\frac{\partial \bar{q}_i}{\partial t}=k_i(q_i^*-\bar{q}_i),\quad k_i=\frac{15D_{ei}}{R_p^2} \quad (6)$$

where k_i is a lumped mass transfer coefficient inside the adsorbent and D_e is the effective diffusivity defined in a homogeneous solid diffusion model (Weber and Chakravort, 1974). q_i^* is the equilibrium amount adsorbed at the bulk gas phase if external film resistance is neglected. The Langmuir−Freundlich isotherm was used to predict the adsorption equilibrium, and this isotherm was extended to predict the multicomponent isotherm by the following loading ratio correlation (LRC) equation (Yang, 1987):

$$q_i=\frac{q_{mi}B_iP_i^{n_i}}{1+\sum_{j=1}^{n}B_jP_j^{n_j}} \quad (7)$$

where the isotherm parameters are functions of temperature:

$$q_m=k_1+k_2T,\quad B=k_3e^{k_4/T},\quad n=k_5+k_6/T \quad (8)$$

The boundary conditions used in the PSA simulation are in the following forms. Boundary conditions for step I (feed pressurization), step II (adsorption), step V (purge), and step VI (pressurizing pressure equalization) are

$$-D_L\left(\frac{\partial y_i}{\partial z}\right)_\alpha=u_\alpha(y_{i,in}-y_{i,\alpha});\quad \left(\frac{\partial y_i}{\partial z}\right)_\beta=0 \quad (9)$$

$$-K_L\left(\frac{\partial T}{\partial z}\right)_\alpha=\rho_g C_{pg}u_\alpha(T_{in}-T_\alpha);\quad \left(\frac{\partial T}{\partial z}\right)_\beta=0 \quad (10)$$

where, for steps I and II, α is $z=0$ and β is $z=L$ and $y_{i,in}=y_{feed}$. For step V, α is $z=L$ and β is $z=0$ and $y_{i,in}$ = time − averaged composition of the effluent stream during step II. For step VI, α is $z=L$ and β is $L=0$ and $y_{i,in}$ = temporal composition of effluent stream during step III.

Boundary conditions for step III (depressurizing pressure equalization) and step IV (depressurization) are

$$\left(\frac{\partial y_i}{\partial z}\right)_{z=0}=\left(\frac{\partial T}{\partial z}\right)_{z=0}=0;\quad \left(\frac{\partial y_i}{\partial z}\right)_{z=L}=\left(\frac{\partial T}{\partial z}\right)_{z=L}=0 \quad (11)$$

In this study, the pressure history obtained during a PSA experiment at the product end was fitted by polynomials used as a boundary condition for the momentum balance. For all the simulations, a clean bed was used as an initial condition:

$$y_i=0 \text{ and } \bar{q}_i=0 \quad \text{at } t=0 \quad (12)$$

Numerical Solution of the Model

A process simulator uses only one bed to simulate this two-bed process. To describe bed connectivities during a pressure equalization step, temporal effluent arrays (flow, pressure, composition, and temperature) from a depressurizing pressure equalization step were retained and used later when the bed underwent a pressurizing pressure equalization step. A finite difference method was used to solve the model equations which consisted of coupled partial differential equations. Fifty nodes in this system were employed to discretize the spatial domain (Hartzog and Sircar, 1995; Kumar, 1994; Yang and Doong, 1985). In order to increase the temporal accuracy of the differential term, a three-point backward method was used except for the first step (Wu et al.,

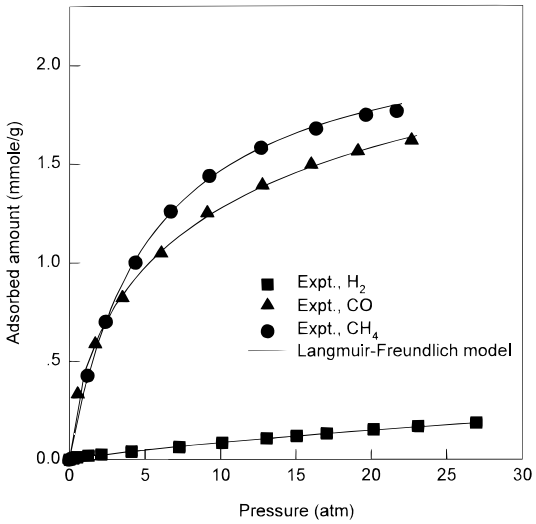

Figure 3. Adsorption isotherms of H_2, CO, and CH_4 at 303 K.

Table 2. Equilibrium Parameters of Langmuir−Freundlich Isotherm

	k_1	k_2	k_3	k_4	k_5	k_6
H_2	4.31	−0.01060	0.002515	458.2	0.9860	43.03
CO	5.05	−0.00905	0.001137	1617.0	0.5245	256.5
CH_4	4.89	−0.00896	0.000534	1795.9	0.396	187.4

1990). Since this method could not be used at the first step, a Crank−Nicholson method was used to maintain the same temporal accuracy.

The required parameters of an adsorption bed and an adsorbent for simulation were listed in Table 1. The uptake curves were measured gravimetrically using electrobalance (Cahn 2000) at 298 K and 0−0.8 atm. These experimental uptake curves were fitted by a homogeneous solid diffusion model to give effective diffusivities. Although these effective diffusivities were increased moderately with an adsorption pressure, average values were used to obtain LDF mass transfer coefficients whose values were 0.587, 0.021, and 0.049 s^{-1} for H_2, CO, and CH_4, respectively. These values were confirmed by breakthrough experiments in previous works (Kim et al., 1995; Yang et al., 1995). Mass and thermal axial dispersion coefficients were estimated to be 6.13 cm^2/s and 4.52×10^{-3} J/K·cm·s, respectively (Suzuki, 1990).

Results and Discussion

Adsorption Isotherms and Heats of Adsorption. Figure 3 shows the adsorption isotherms of H_2, CH_4, and CO on zeolite 5A at 303 K and 0−25 atm. As expected, the results showed very high selectivity for CO and CH_4 over H_2 at the range of experimental temperature. The CH_4 isotherm and CO isotherm cross over at about 2.5 atm. Although the adsorption capacity of H_2 is very small, H_2 is treated as an adsorbable component in this study. The pure isotherm data fitted very well to the Langmuir−Freundlich isotherm model. The parameters for eq 8 were obtained from the adsorption isotherms under three different temperature conditions, and they are shown in Table 2.

Since the heat of adsorption is a good measure for calculating the strength of the interaction between the adsorbates and adsorbent and for checking the temperature change in a bed, the isosteric heat of adsorption was calculated by using the Clausius−Clapeyron equation and is represented in Figure 4. As shown in the figure, while the adsorption heat of hydrogen is very low, the heat of adsorption of CO or CH_4 is relatively very high. Therefore, hydrogen can be said to interact very weakly on zeolite compared to other components. Generally, since the higher the heat of adsorption, the stronger the adsorption is, it is difficult to complete desorption through depressurization and the swing range of temperature becomes larger due to the heat of adsorption. Therefore, it affects the process performance in a negative manner. As shown in Figure 4, the actual heat of adsorption should be in relation to the adsorption quantity, but in this study constant values of 2800, 5000, and 5300 cal/mol in the simulation were used for H_2, CO, and CH_4, respectively.

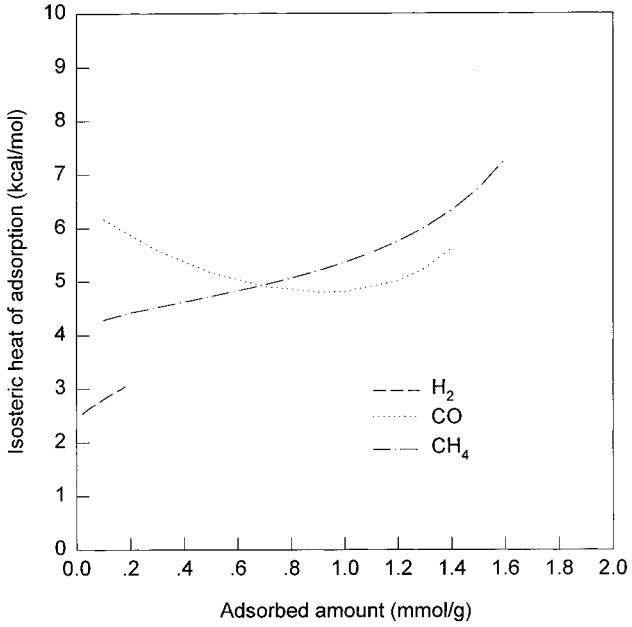

Figure 4. Isosteric heat of adsorption of H_2, CO, and CH_4.

The adsorbent used in this study showed slightly smaller adsorption capacities than that of Chen et al. (1990). Especially, in contrast with this study, CO exhibited a slightly larger adsorption capacity than that of CH_4. In case of heats of adsorption, both studies showed similar average values, while an increase in the heat of adsorption with a loading of H_2 and CH_4 was opposite to their result. It can be interpreted as strong effects of adsorbate−adsorbate interaction on the apparent heat of adsorption in the case of the adsorbent used in this study (Valenzuela and Myers, 1989). Generally, because there are many factors, such as binder and exchanged cations, affecting adsorption isotherms, different isotherms can be obtained even for the same type of an adsorbent.

PSA Performance. According to the simulation, after approximately 10 cycles, the difference between the performances of the 2 latest cycles were less than 0.01% and this was experimentally confirmed up to 30 cycles. In this study, all the experimental data were collected at above 15 cycles.

Several operating parameters were changed to study the effects of these parameters on PSA performance, and experimental conditions were described in Table 3.

The hydrogen concentration of the effluent at each step of the PSA cycle at run C′ in Table 3 is shown in Figure 5 along with experimental values. The hydrogen concentration of the effluent was measured at the product end during the adsorption step and at the feed end during the countercurrent depressurization step

Table 3. Operation Conditions for Experimental Run[a]

run		step time (s)						adsorption pressure (atm)	purge rate (L/min)	*P/F* ratio[b]
H_2/CO	H_2/CH_4	I	II	III	IV	V	VI			
	run A′	30	180	40	30	180	40	6	0.22	0.11
run B	run B′	30	180	40	30	180	40	9	0.22	0.11
run C	run C′	30	180	40	30	180	40	11	0.22	0.11
run D	run D′	30	180	40	30	180	40	13	0.22	0.11
run E	run E′	30	180	40	30	180	40	16	0.22	0.11
run F		30	180	40	30	180	40	11	0.10	0.05
	run G′	30	180	40	30	180	40	11	0.15	0.075
run H	run H′	30	180	40	30	180	40	11	0.35	0.175
	run I′	30	240	40	30	240	40	11	0.22	0.11
	run J′	30	300	40	30	300	40	11	0.22	0.11
run K		30	180	5	30	180	5	11	0.22	0.11
run L		30	180	20	30	180	20	11	0.22	0.11

[a] Feed rate was set to 2 L/min for all the runs. [b] *P/F* ratio = amount of H_2 used in purge step/amount of H_2 inlet in adsorption step.

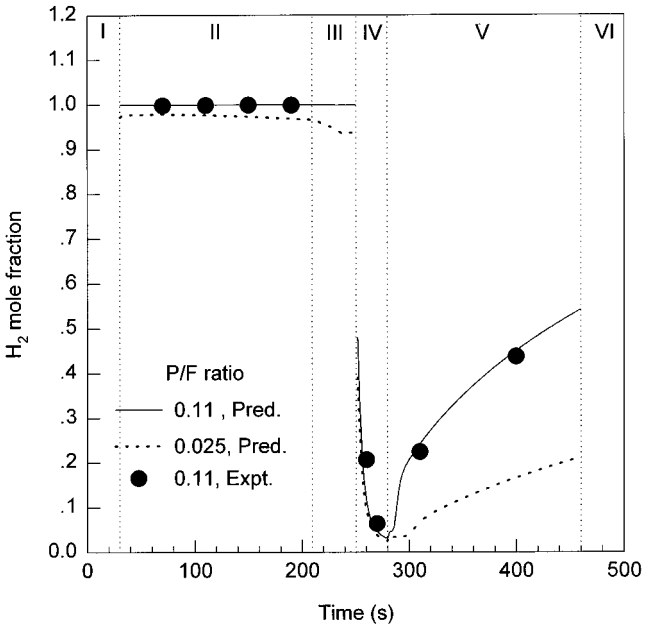

Figure 5. H_2 mole fraction of an effluent stream for run C′ with a 0.11 or 0.025 *P/F* ratio.

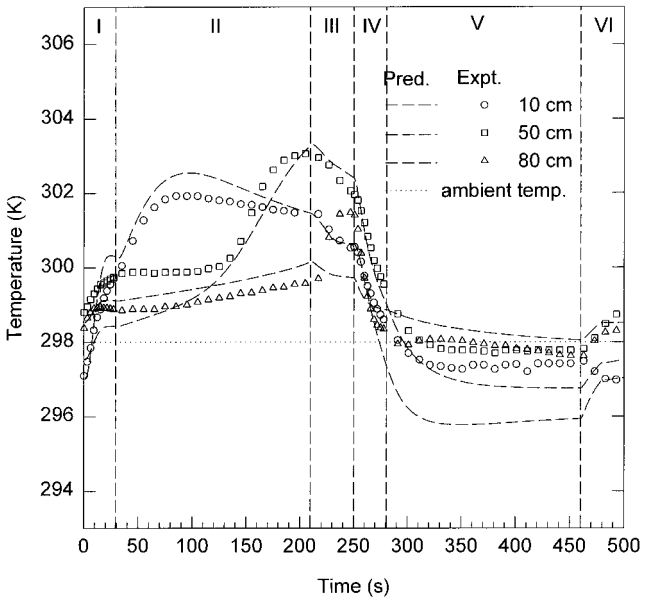

Figure 6. Temperature variations with time at various points along the bed for run C.

and the purge step. As shown in Figure 5, considering the complexity of the process, the calculated values using a mathematical model predicted the behavior of all the steps in PSA fairly well. This, together with temperature profiles in the bed, helps justify the results of simulation that predict the dynamic behavior of an adsorption bed in a situation where it is difficult to actually measure the concentration in a bed.

In this figure, at the pressure equalization step, the hydrogen concentration of the effluent at the product end under the 0.11 *P/F* ratio in Figure 5 did not differ greatly from product purity. However, as can be seen at the *P/F* ratio of 0.025, the effluent gas of low hydrogen purity during the depressurizing pressure equalization step was used to partially pressurize the product end of the regenerated bed. And this was because of a little amount of purge. Therefore, the product end is contaminated by strong adsorbates. This lowers the purity of the product at the beginning of the adsorption steps and affects the whole product purity.

When the results of a two-bed PSA using zeolite 5A were compared with those of a one-bed PSA system from the previous work (Yang et al., 1995), the purity of H_2 was increased from 97.7% to 99.99% in the H_2/CO system. However, the recovery of H_2 was greatly improved around 10−20% due to the pressure equalization step in a two-bed PSA system. Also, the recovery of H_2 in the two-bed PSA system was more sensitively affected by the operating conditions such as the adsorption pressure and *P/F* ratio than that in a one-bed PSA system.

Figure 6 shows temperature variations at three different locations in a bed in the H_2/CO system during run C. As can be seen from this figure, even though the amount of feed gas was not large and the bed's diameter was much smaller than its length in comparison with a commercial unit, the swing range of the temperature reached about 5 K in the experiment. Since the peak in the figure indicates the thermal wave front associated with adsorption, the concentration front has passed the midpoint of the bed in the middle of the adsorption step. The desorption of CO occurred in the bed during a pressure equalization step, but only in a slight amount. Further desorption in blowdown and purge steps was also indicated by the continuous decline in temperature. The temperature variation was well predicted at each step of the PSA process through a mathematical model simulation. However, the temperature variation in the simulated results was greater than that in the experimental results, and it was more apparent at the bed entrance during a desorption step.

(i) Effects of Adsorption Pressure. Figure 7 shows the effect of an adsorption pressure on performance for H_2/CH_4 and H_2/CO systems under a 0.22 L/min purge rate. The H_2 purity declines rapidly below

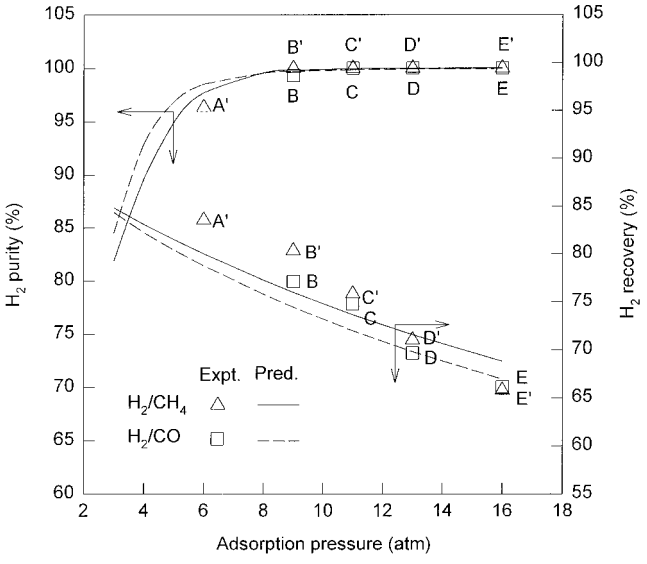

Figure 7. Effects of adsorption pressure on H_2 purity and recovery for H_2/CO and H_2/CH_4 systems under a 0.22 L/min purge rate. (The symbols of relevant runs are specified alphabetically in Table 3.)

about 8 atm for both systems while recovery declines almost linearly with pressure. The decline of recovery is mostly due to the loss of H_2 in the feed end during countercurrent depressurization. In general, the greater the number of pressure equalization steps that were involved during a complete PSA cycle, the lower the loss of gases that vented in the atmosphere. Therefore, when the operating pressure ratio is high, it is desirable to incorporate many adsorption beds in order to obtain good recovery. However, it will increase the capital cost. As shown in the figure, the purity of hydrogen crossed over around 8 atm. And higher H_2 purity was shown in the H_2/CH_4 system at high pressure and in H_2/CO system at low pressure. Considering the partial pressure of the feed (2.4 atm), this agrees with the cross pressure of adsorption isotherms of CO and CH_4. The recovery in the H_2/CH_4 system was a little higher than that in the H_2/CO system.

Figure 8 shows the predicted axial profiles of the H_2 mole fraction in the gas phase at the end of the adsorption step. Since the slope of the mass-transfer zone (MTZ) becomes steeper at higher pressure, beds can be used more effectively and at the same time the purity of the product becomes higher. But, the difference between concentration profiles becomes smaller as pressure becomes higher than 11 atm. This is because the adsorption isotherm converges to the limiting adsorption amount at high pressure. Therefore, the bed efficiency is not so good above certain pressure points, and recovery falls down continuously (Figure 7). Figure 9 shows the quantity of the adsorbed CH_4 in the adsorbed phase. If higher pressure is applied, the adsorption capacity becomes greater and the breakthrough time becomes longer. However, at above 11 atm, there is not so much elongation effect of the loading pattern compared to that at 11 atm. This implies that it has come near the maximum amount of adsorption at the equilibrium. When the adsorption pressure is low, the whole packed bed becomes saturated very quickly and adsorption lessens at the product end. Therefore, the purity of H_2 goes down.

(ii) Effects of the *P/F* Ratio. Figure 10 shows a performance change of H_2/CH_4 and H_2/CO separation at 11 atm as different purge amounts, namely the *P/F*

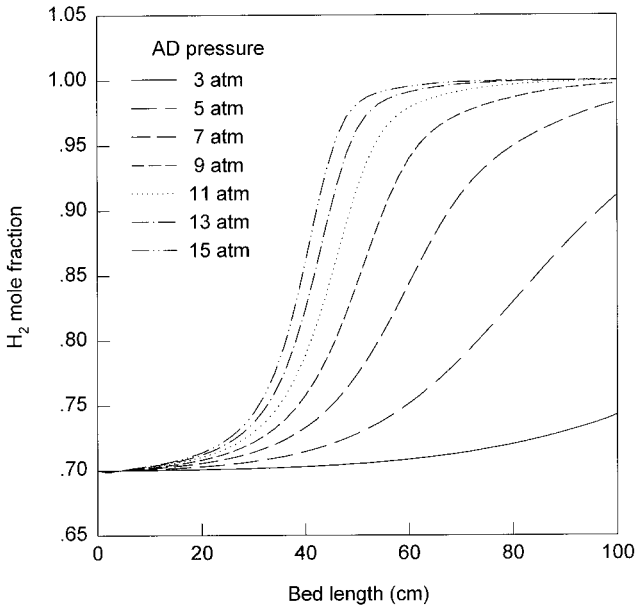

Figure 8. Effects of adsorption pressure on axial profiles of an H_2 mole fraction in the gas phase at the end of the adsorption step for the H_2/CH_4 system.

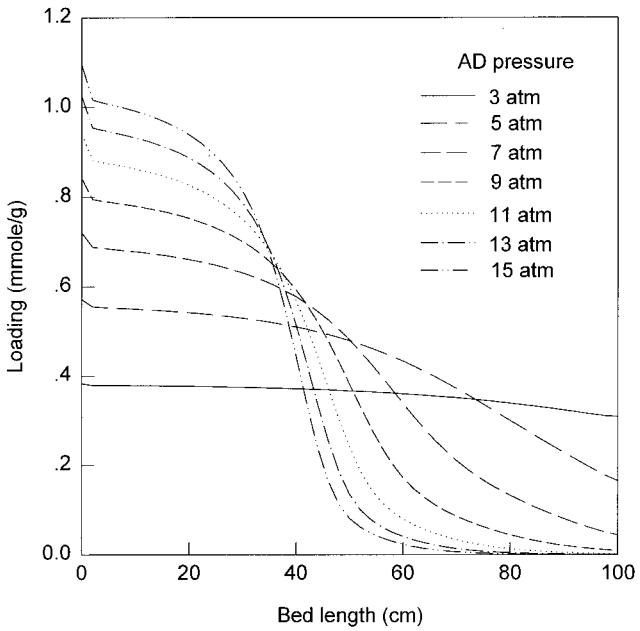

Figure 9. Effects of adsorption pressure on axial profiles of the adsorbed amount of CH_4 at the end of the adsorption step for the H_2/CH_4 system.

ratio, are used. The *P/F* ratio is defined as a ratio of the amount of H_2 used in a purge step to that fed in an adsorption step, as Yang and Doong (1985) has defined. Similar to a general case, as the *P/F* ratio was increased the purity of H_2 in the product increased, but the purity of strong adsorbates decreased because of the dilution by the purge stream. The increase in product purity with the *P/F* ratio in an asymptotic manner levels off above 0.07 in the *P/F* ratio in both systems. Especially, when the purge amount is smaller than this, the purity of H_2 was expected to go down more drastically in the H_2/CH_4 system rather than in the H_2/CO system. However, such an effect was not so great as that of the adsorption pressure in Figure 7. Both H_2/CO and H_2/CH_4 systems declined greatly in recovery over the full range of the *P/F* ratio. And recovery was always higher in the H_2/CH_4 system than in the H_2/CO system.

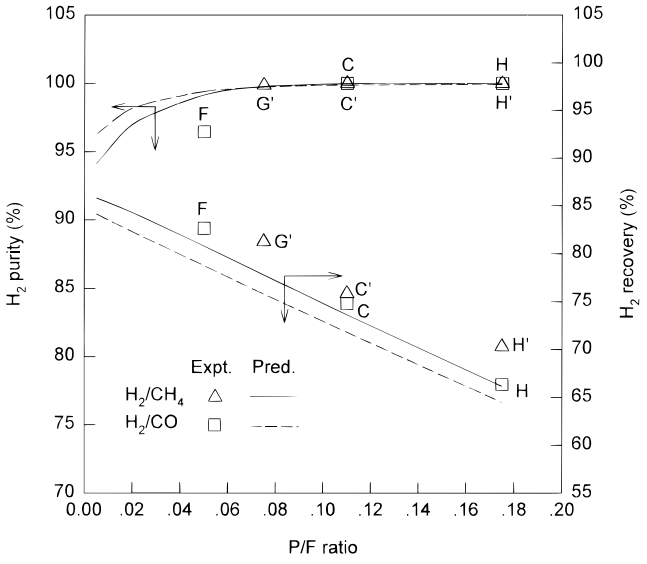

Figure 10. Effects of the *P*/*F* ratio on H_2 purity and recovery for H_2/CO and H_2/CH_4 systems at an adsorption pressure of 11 atm. (The symbols of relevant runs are specified alphabetically in Table 3.)

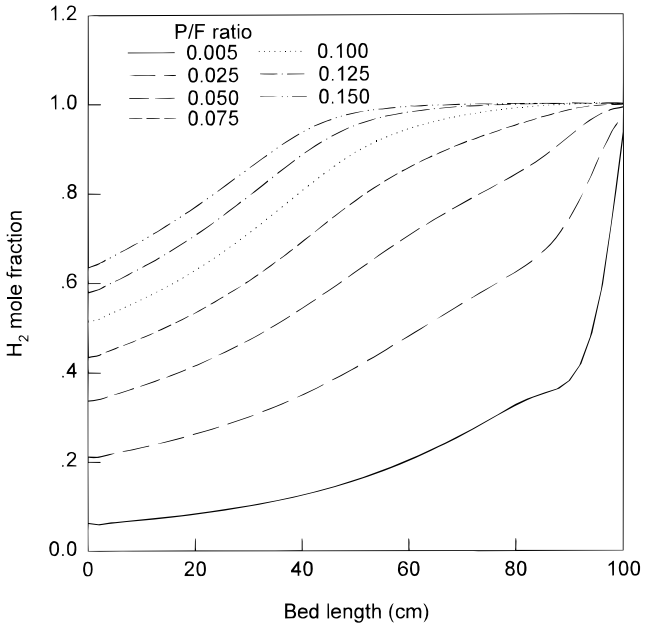

Figure 11. Effects of the *P*/*F* ratio on axial profiles of the H_2 mole fraction at the end of a purge step for the H_2/CH_4 system.

This *P*/*F* ratio effect is more clearly demonstrated by concentration profiles in the bed at the end of a purge step. Figures 11 and 12 show the H_2 concentration profile in the gas phase and the adsorbed amount of CH_4 in the adsorbed phase, respectively. The greater the purge amount, the larger the H_2 concentration from the product end of the bed and the faster the desorption of CH_4 at the adsorbed phase. At the range of 0.05 and 0.075 in the *P*/*F* ratio in Figure 11, the slope of the H_2 concentration profile at the product end was changed from a concave to an asymptotic manner. At the small purge rate, while the purge step affects the concentration profile mostly at the product end, the shape of the concentration profile of a depressurization step is more or less kept at the other part of the bed. However, above 0.075 in the *P*/*F* ratio which shows the asymptotic MTZ at the product end, the effect of the purge amount became small. Therefore, to obtain high purity of H_2,

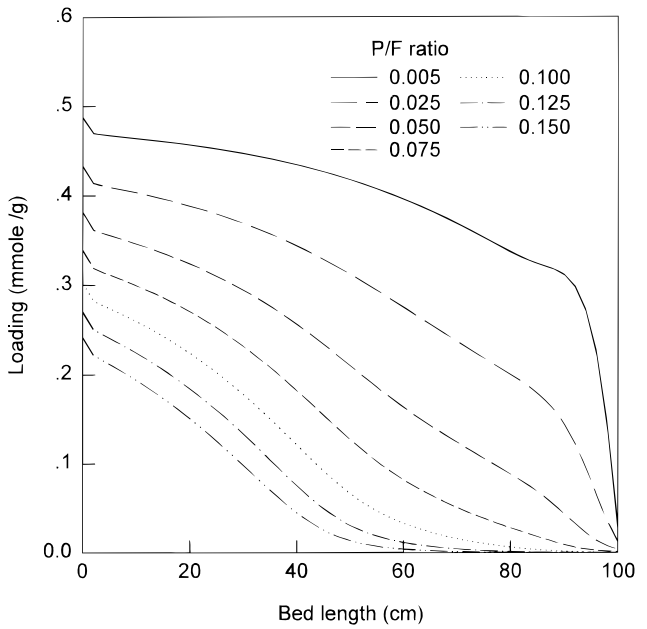

Figure 12. Effects of the *P*/*F* ratio on axial profiles of the adsorbed amount of CH_4 at the end of a purge step for the H_2/CH_4 system.

the purge rate should be large enough to remove the effects of a previous step, the depressurization step, in both gas and adsorbed phases. In the case of this study, the *P*/*F* ratio around 0.075 can meet this criterion. However, to obtain more than 99.99% high purity in the experimental range of this study, the *P*/*F* ratio should be higher than 0.075. It is also verified in Figure 10 in which H_2 purity drops steeply in this region.

The effects of the *P*/*F* ratio were studied by many researchers. Cen and Yang (1986) obtained 99.99% purity of H_2 with about 66% recovery under the operating conditions of 21.4 atm of adsorption pressure, 31.9 LSTP/min feed rate, and a 0.092 *P*/*F* ratio for the one-bed PSA process using the activated carbon in the H_2/CO system, when only the effluent of step II was taken as a product in their study. Yang and Doong (1985) studied H_2/CH_4 separation using the same apparatus and adsorbent as those in Cen and Yang's work (1986) with different step times. In their work, purity was reached to 98.9% with a recovery of about 46%. Kumar (1994) did a numerical study on the separation of the H_2/CH_4 mixture by using a four-bed H_2 PSA with a Ca-exchanged zeolite and attained over 99.999% purity and about 85% of recovery. As an example of a commercial H_2 PSA process, the Air Products PSA process produces 99.999+% H_2 purity with 85+% recovery (Ruthven et al., 1994). It consists of two groups of adsorbers which have six and three adsorbers, respectively. Therefore, it can be seen that both purity and recovery increase with an increasing number of beds due to a small amount of waste gas and gradual pressurization with light product rich gas. It can also be found that the purity and recovery from this study are between the corresponding performances of one-bed and four-bed PSA processes.

(iii) Effects of Adsorption Step Time and Purge Condition. To investigate the relative importance of a *P*/*F* ratio in the PSA process, various combinations of the *P*/*F* ratio were applied to the H_2/CH_4 and H_2/CO systems in the zeolite 5A PSA system. The model simulation and experimental results of the effects of adsorption step time under various purge conditions are presented in Figure 13. In Case I, the effect of the

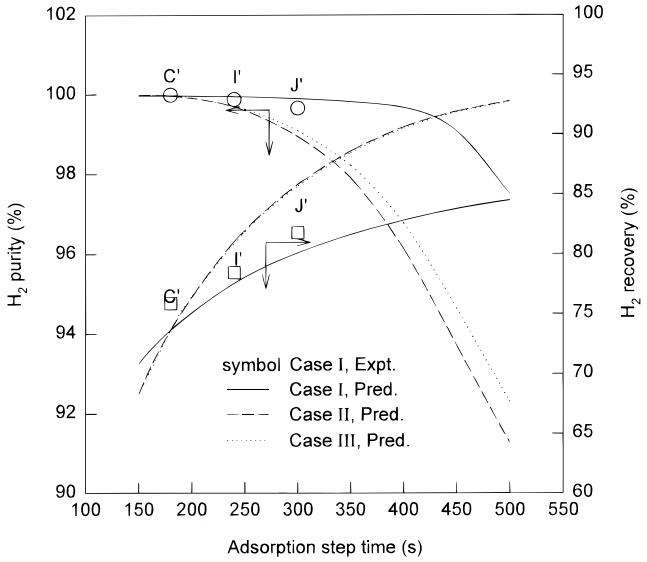

Figure 13. Effects of the adsorption step time on H_2 purity and recovery depending on several purge conditions for the H_2/CH_4 system (adsorption pressure: 11 atm). Case I: 0.22 L/min of purge rate with purge step time equal to the adsorption step time. Case II: 0.22 L/min of purge rate with fixed purge step time, 180 s (0.66 L). Case III: 0.66 L of purge of gas amount with purge step time equal to adsorption step time. (The symbols of relevant runs are specified alphabetically in Table 3.)

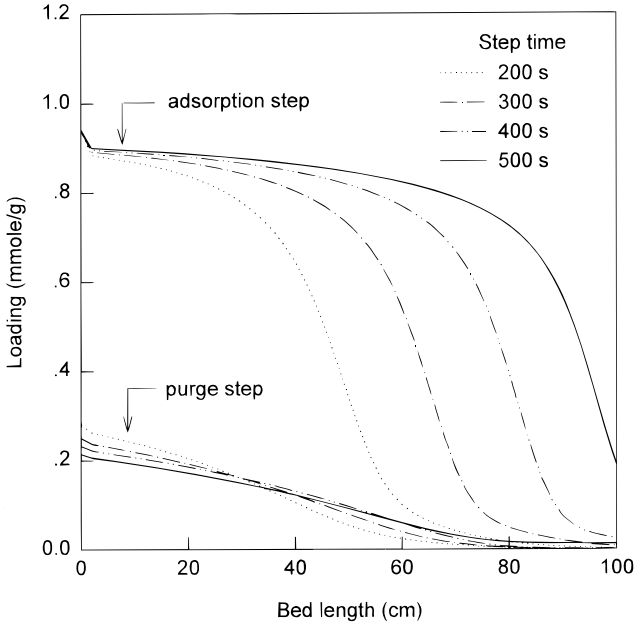

Figure 14. Axial profiles of the adsorbed amount of CH_4 at the end of the adsorption and purge steps depending on the adsorption and purge step time for the H_2/CH_4 system.

adsorption step time was studied under the same step time for the adsorption and purge steps at the purge rate of 0.22 L/min in the H_2/CH_4 system. Since the duration of the purge step was increased with an increase in the adsorption step time, the same *P*/*F* ratio was used for all the experimental data of this figure. Despite a great range of time changes for adsorption and purge steps, it was impressive that the purity of hydrogen was not affected so much and recovery increased with step time. As a result, the productivity of adsorbents will increase. Therefore, this result showed that it is possible to obtain different performances and productivity of adsorbents with the same *P*/*F* ratio. Such a phenomenon can be verified in Figure 14. The concentration of CH_4 in the adsorbed phase after the purge step did not change much with step time, but there was a great difference in the loading amount after the adsorption step. Regardless of the adsorption and purge step times, almost complete regeneration occurred at the product end. On the other hand, at the feed end, even though the amount of the adsorbed CH_4 became large under the long step time of the adsorption step, almost the same amount of CH_4 remained at the feed end when the purge step was finished. On the other hand, in Case II (in Figure 13), the effect of the adsorption step time was studied with the same feed rate as that of Case I and a fixed purge step time of 180 s. As shown in the figure, as the adsorption step time was increased, there was an increase in recovery while the product purity decreased drastically. Therefore, mere lengthening of the adsorption step time for the sake of increasing the productivity of the adsorbents without an increase in purge amount resulted in worse performance. In Case III, the same adsorption step time and purge step time as in Case I were used, while the same amount of purge (0.66 L) as in Case II was used. In this case, recovery should be the same as that of case II. However, even though the same amount of purge (or *P*/*F* ratio) was used at certain adsorption step time, the longer the purge step times, a little higher the purity of hydrogen that was obtained in Case III than in Case II. This indicates that a certain period of time is needed for CH_4 desorption.

As a result, it can be said that a proper step time and flow rate in a purge step can be changed according to various process variables, and that the *P*/*F* ratio alone is not enough to explain a purge step.

(iv) Effects of Pressure Equalization Time. Although the pressure equalization step is a typical step in a multibed PSA process and plays a key role in improving the PSA performance, this step has not been widely studied in spite of its importance. As the main purpose of the pressure equalization step is to avoid wasteful vent of gas in void of an adsorption bed and, thus, to lower the power consumption required to compress feed gas, this goal can be attained by only a simple connection between two adsorption beds. However, the gas in the void fraction of the product end part is a light product-concentrated gas and also has a concentration gradient made during a previous adsorption step. Therefore, the duration of pressure equalization time or the direction of gas flow can more or less affect the PSA performance.

An extended and profound research of the pressure equalization step can be found in the U.S. Patent of Tagawa et al. (Tagawa et al., 1988). In this patent, four kinds of methods to achieve pressure equalization were investigated, but the effect of the duration of the step was not considered. On the other hand, Lemcoff et al. (1992) studied pressure equalization time in kinetic air separation using a carbon molecular sieve. In their study, a longer pressure equalization step time gave much more specific product and nitrogen yield.

In this study, the effects of the duration of the pressure equalization step were investigated in H_2 PSA in which the equilibrium effect dominates the separation. As shown in Table 3, three pressure equalization step times (5, 20, and 40 s) were applied to the PSA cycle. In Figure 15, the longer the step time, the better purity and recovery were obtained. However, after a certain period of time for the pressure equalization step, purity and recovery were not affected by this step time. This might be explained by the fact that for equilibrium

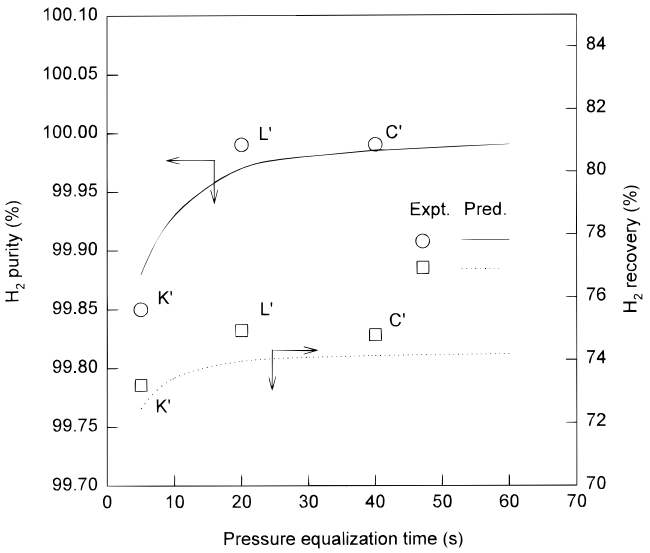

Figure 15. Effects of pressure equalization time on H_2 purity and recovery for the H_2/CH_4 system. (The symbols of relevant runs are specified alphabetically in Table 3.)

separation, the gas that was moved to the regenerated bed needs some degree of time to adsorb impurity before being pushed back to the product end by a pressurized feed gas at the feed pressurization step. Therefore, it can be said that if the pressure equalization step is too fast, it has a bad effect on the performance.

Conclusion

It was possible to obtain hydrogen of over 99.99% purity with 75% recovery in the H_2/CO system and 80% recovery in the H_2/CH_4 system by a two-bed six-step PSA process using zeolite 5A as an adsorbent from the hydrogen mixtures of 30 vol % CO or CH_4. With an application of the pressure equalization step in the two-bed PSA system, there showed a great improvement in recovery but only a slight increase in purity, as compared with the one-bed PSA system.

When the adsorption pressure or *P*/*F* ratio increased, the purity of the H_2 product and the recovery of strong adsorbates product increased. The effect of the adsorption pressure was more crucial than that of the *P*/*F* ratio for purity. As high purity of H_2 (99.99%) was obtained under a certain *P*/*F* ratio, the concentration profile of H_2 showed an asymptotic approach at the product end.

The hydrogen purity dropped only a little through the lengthening of both the adsorption and purge step times under the same *P*/*F* ratio. Also, despite the same purge amount at the purge step, lengthening the purge step time resulted in better purity of hydrogen. Certain elongation of pressure equalization step time also improved a PSA performance at the expense of adsorbent productivity. All of these results showed that it was also important to study the effects of step times as well as the role of each step in the equilibrium separation. The experimental data of a two-bed PSA cycle could be simulated by a model incorporating LRC, heat and momentum balances, and an LDF model.

Acknowledgment

The financial assistance and support of R&D Management Center for Energy and Resources is gratefully acknowledged.

Nomenclature

A = cross sectional area, cm^2
B = Langmuir−Freundlich isotherm parameter, atm^{-1}
C_p = heat capacity, cal/g·K
D_L = mass axial dispersion coefficient, cm^2/s
K_L = thermal axial dispersion coefficient, cal/K·cm·s
k_i = mass transfer coefficient for LDF model, s^{-1}
n = Langmuir−Freundlich isotherm parameter
P = pressure, atm
q = adsorbed amount, mol/g
q_m = Langmuir-Freundlich isotherm parameter, mol/g
$\bar{q}$ = volume-averaged amount adsorbed in an adsorbent, mol/g
Q = average isosteric heat of adsorption, cal/mol
R = radius, cm
STP = standard temperature and pressure
t = time, s
T_{atm} = ambient temperature, K
T = pellet or gas temperature, K
u = interstitial velocity, cm/s
h = heat transfer coefficient, cal/cm^2·K·s
y = mole fraction in bulk gas phase
z = axial position in the bed, cm

Greek Letters

α = total void fraction
ϵ = interparticle void fraction
ρ = density, cm^3/g
μ = viscosity, cm/g·s

Subscripts

B = bed
i = species i
p = adsorbent pellet
g = gas phase
s = solid phase
w = wall

Superscript

* = equilibrium

Literature Cited

Cen, P.; Yang, R. T. Bulk Gas Separation by Pressure Swing Adsorption. *Ind. Eng. Chem. Fundam.* **1986**, *25*, 758.

Chen, Y. D.; Ritter, J. A.; Yang, R. T. Nonideal Adsorption from Multicomponent Gas Mixtures at Elevated Pressure on a 5A Molecular Sieve. *Chem. Eng. Sci.* **1990**, *45*, 2877.

Chlendi, M.; Tondeur, D. Dynamic Behaviour of Layered Columns in Pressure Swing Adsorption. *Gas. Sep. Purif.* **1995**, *9*, 231.

Doong, S. J.; Yang, R. T. Bulk Separation of Multicomponent Gas Mixtures by Pressure Swing Adsorption: Pore/Surface Diffusion and Equilibrium Models. *AIChE J.* **1986**, *32*, 397.

Doong, S. J.; Yang, R. T. Bidisperse Pore Diffusion Model for Zeolite Pressure Swing Adsorption. *AIChE J.* **1987**, *33*, 1045.

Hartzog, D. G.; Sircar, S. Sensitivity of PSA Process Performance to Input Variables. *Adsorption* **1995**, *1*, 133.

Kim, W.-G.; Yang, J.; Han, S.; Cho, C.; Lee, C.-H.; Lee, H. Experimental and Theoretical Study on H_2/CO_2 Separation by a Five-Step One-Column PSA Process. *Korean J. Chem. Eng.* **1995**, *12*, 503.

Kumar, R. Pressure Swing Adsorption Process: Performance Optimum and Adsorbent Selection. *Ind. Eng. Chem. Res.* **1994**, *33*, 1600.

Lemcoff, N. O.; Doong, S. J.; LaCava, A. I. Modeling of Equalization in Air Separation by Pressure Swing Adsorption. Proc. The 4th International Conferences on Fundamentals of Adsorption, Kyoto, Japan, May, 1992.

Ruthven, D. M.; Farooq, S.; Knaebel, K. S. *Pressure Swing Adsorption*; VCH Publishers: New York, 1994.

Suzuki, M. *Adsorption Engineering*; Kodansha: Tokyo, 1990.

Tagawa, T.; Suzu, Y.; Hayashi, S.; Mazuguchi, Y. Enrichment in Oxygen Gas. U.S. Patent No. 4,781,735, 1988.

Valenzuela, D. P.; Myers, A. L. *Adsorption Equilibrium Data Handbook*; Prentice Hall: London, 1989.

Weber, T. W.; Chakravort, R. K. Pore and Solid Diffusion Models for Fixed-bed Adsorbers. *AIChE J.* **1974**, *20*, 228.

Wu, J. C.; Fan, L. T.; Erickson, L. E. Three-point Backward Finite-difference Method for Solving a System of Mixed Hyperbolic-parabolic Partial Differential Equations. *Comput. Chem. Eng.* **1990**, *14*, 679.

Yang, R. T. *Gas Separation by Adsorption Processes*; Butterworths: Boston, 1987.

Yang, R. T.; Doong, S. J. Gas Separation by Pressure Swing Adsorption: A Pore-Diffusion Model for Bulk Separation. *AIChE J.* **1985**, *31*, 1829.

Yang, J.; Han, S.; Cho, C.; Lee, C.-H.; Lee, H. Bulk Separation of Hydrogen Mixtures by a One-column PSA Process. *Sep. Technol.* **1995**, *5*, 239.

Received for review November 14, 1996
Revised manuscript received April 1, 1997
Accepted April 9, 1997[⊗]

IE960728H

[⊗] Abstract published in *Advance ACS Abstracts,* June 1, 1997.